NANO · MICRO small
www.small-journal.com

Ratiometric Nanothermometer Based on a Radical Excimer for In Vivo Sensing

Davide Blasi, Nerea Gonzalez-Pato, Xavier Rodriguez Rodriguez, Iñigo Diez-Zabala, Sumithra Yasaswini Srinivasan, Núria Camarero, Oriol Esquivias, Mònica Roldán, Judith Guasch, Anna Laromaine, Pau Gorostiza, Jaume Veciana, and Imma Ratera**

Ratiometric fluorescent nanothermometers with near-infrared emission play an important role in in vivo sensing since they can be used as intracellular thermal sensing probes with high spatial resolution and high sensitivity, to investigate cellular functions of interest in diagnosis and therapy, where current approaches are not effective. Herein, the temperature-dependent fluorescence of organic nanoparticles is designed, synthesized, and studied based on the dual emission, generated by monomer and excimer species, of the tris(2,4,6-trichlorophenyl) methyl radical (TTM) doping organic nanoparticles (TTMd-ONPs), made of optically neutral tris(2,4,6-trichlorophenyl)methane (TTM-αH), acting as a matrix. The excimer emission intensity of TTMd-ONPs decreases with increasing temperatures whereas the monomer emission is almost independent and can be used as an internal reference. TTMd-ONPs show a great temperature sensitivity (3.4% K^{-1} at 328 K) and a wide temperature response at ambient conditions with excellent reversibility and high colloidal stability. In addition, TTMd-ONPs are not cytotoxic and their ratiometric outputs are unaffected by changes in the environment. Individual TTMd-ONPs are able to sense temperature changes at the nano-micro-scale. In vivo thermometry experiments in *Caenorhabditis elegans* (*C. elegans*) worms show that TTMd-ONPs can locally monitor internal body temperature changes with spatio-temporal resolution and high sensitivity, offering multiple applications in the biological nanothermometry field.

1. Introduction

Nanothermometry is becoming a fundamental topic in several technological and scientific fields like electronics and biology.[1–6] Indeed, the miniaturization and the increment in power density in micro and optoelectronic devices require accurate temperature determination with high spatial resolution of the thermal effects (self-heating, heat dissipation, etc.) to optimize device performance.[1–4] In biology, during the last years a rising interest in intracellular thermal sensing has appeared,[5–7] for instance in diagnosis (sensing the heat production in cancer and inflammatory processes)[8,9] and in hyperthermia therapy, where monitoring the temperature during the treatment is fundamental to avoid an over-generation of heat that can burn the surrounding tumor's tissue.[10–12] Nanothermometry for biology is still challenging since bio-sensors should exhibit high sensitivity, accuracy, and spatial resolution, together with

D. Blasi, N. Gonzalez-Pato, X. Rodriguez Rodriguez, I. Diez-Zabala, S. Y. Srinivasan, O. Esquivias, J. Guasch, A. Laromaine, J. Veciana, I. Ratera
Institut de Ciència de Materials de Barcelona (ICMAB-CSIC)
Bellaterra 08193, Spain
E-mail: vecianaj@icmab.es; iratera@icmab.es

D. Blasi
Dipartimento di Chimica
Università degli Studi di Bari "Aldo Moro"
Bari 70125, Italy

N. Gonzalez-Pato, X. Rodriguez Rodriguez, J. Guasch, P. Gorostiza, J. Veciana, I. Ratera
Networking Research Center on Bioengineering
Biomaterials and Nanomedicine (CIBER-BBN)
Campus UAB
Bellaterra 08193, Spain

The ORCID identification number(s) for the author(s) of this article can be found under https://doi.org/10.1002/smll.202207806.

DOI: 10.1002/smll.202207806

N. Camarero, P. Gorostiza
Institute for Bioengineering of Catalonia (IBEC)
The Barcelona Institute of Science and Technology
Clúster, Baldiri Reixac 10-12, Barcelona 08028, Spain

M. Roldán
Unitat de Microscòpia Confocal i Imatge Cellular
Servei de Medicina Genètica i Molecular
Institut Pediàtric de Malaties Rares (IPER)
Hospital Sant Joan de Déu
Esplugues de Llobregat 08950, Spain

J. Guasch
Dynamic Biomimetics for Cancer Immunotherapy
Max Planck Partner Group
ICMAB-CSIC
Campus UAB
Bellaterra 08193, Spain

P. Gorostiza
Catalan Institution for Research and Advanced Studies (ICREA)
Barcelona 08010, Spain

no cytotoxicity and optical and colloidal stabilities being such properties unaffected by changes in pH, concentration, ionic strength, and viscosity typical affecting biological media.[13] Several systems have been explored as nanothermometers meeting all these requirements, such as organic molecular dyes,[14,15] quantum dots (QDs),[16] Ln^{3+} doped systems,[10,17,18] polymers, and hybrid organic-inorganic systems.[19–22] All these luminescent sensors exploit the thermal dependence of a fluorophore emission for determining the temperature. These changes can be observed as variations in luminescence intensity, emission band shape, polarization, lifetime, or broadening of the emission bandwidth.[23]

Intensity-based sensors offer the possibility to work with a simple set-up,[24] reducing costs and time for data analysis.[25] Despite its simplicity, an absolute emission intensity measurement can lead to errors due to fluctuations in the active fluorophore concentration inside the cell or tissue due to aggregation or photodegradation. To overcome these problems, a ratiometric output with a dual emission sensing system is needed, also called luminescent intensity ratio (LIR). The simplest strategy, in order to have a dual emission, is to bind together two different emitting species with different thermal quenching of the emission, or exploit different states of aggregation of the same fluorophore, like in the case of excimers.[12,15,24,26,27]

Recently, organic nanoparticles (ONPs)[28] and radical-based ONPs have been proposed as fluorescence probes for in vitro bioimaging.[29] Indeed, polyhalogenated trityl radicals can achieve long-wavelength emission without the need of an extended conjugated system.[30,31] In addition, it is possible to further red-shift radical emission into the biological transparency window (650 – 950 nm) through the formation of excimers. These excimers, obtained by dispersing radical species in rigid hosts (generally the closed-shell radical precursor) have been studied during the last years due to the possibility to modulate their association/dissociation via the application of an external magnetic field at liquid helium temperature.[32,33] However, tuning the radical excimer association/dissociation by varying the external temperature has never been reported.

In this work, we propose a highly sensitive full-organic contactless nanothermometer based on organic radical nanoparticles (TTMd-ONPs) consisting of the optically neutral tris(2,4,6-trichlorophenyl)methane (TTM-αH) as a matrix and the tris(2,4,6-trichlorophenyl)methyl radical (TTM) as dopant (**Figure 1**). These nanoparticles exhibit a dual emission due to the presence of radical monomers and excimers inside the particle. Increasing temperatures cause a decrease in the excimer emission intensity without a significant alteration of the monomer emission, which allows to use it as an internal reference. This system offers a simple and reproducible nanoscopic sensor, entirely based on two small metal-free molecules, the open-shell TTM radical and its close-shell precursor, the TTM-αH, which are processed as TTMd-ONPs in a single-step self-assembly process, using the re-precipitation method. Achieving a ratiometric output using excimers instead of two different emitting species simplifies and optimizes the preparation of the nano-sensor as well as the thermal sensing, since both emissions come from the same compound and thus, a single wavelength can excite both emitting species. Thus, no correction for different bleaching rates is needed as in the case of hybrid systems. Moreover, excimers of the TTMd-ONPs emit in the region of deep-red/near infrared (NIR) (the first transparency windows of biological tissues), offering the opportunity to penetrate in the deep-tissue for in vivo applications.[34] In addition, TTMd-ONPs, owing to their metal-free formulation, are non-cytotoxic and their ratiometric outputs are unaffected by changes in pH and ionic strength that may occur under physiological conditions. Moreover, thanks to the magnetic properties of the TTMd-ONPs, could also be used as dual-mode bioimaging, coupling luminescence, and magnetic resonance.[35]

2. Results and Discussion

In previous works, we reported, for the first time, that TTM radical was able to form excimers when dispersed in rigid matrices (polymers or ONPs), like in TTMd-ONPs.[36,37] Radical excimers in ONPs are extremely promising since they are efficient emitters in the NIR, constituting an attractive system for optoelectronics.[32,33] These TTMd-ONPs were characterized by an average size distribution of ≈100 nm, spherical shape, and high colloidal stability in water. In addition, these radical doped systems can also play a relevant role in bio-imaging and bio-sensing since they are water dispersible and present unique optical properties. Indeed, they show a huge Stock's shift and an efficient emission in the first biological transparency window (650 – 950 nm), which minimizes self-absorption effects and shows better tissue penetration compared to UV-visible wavelengths,[38] together with microsecond lifetimes that allow filtering self-fluorescence signals simply applying a delay between excitation and detection. Therefore, the optical

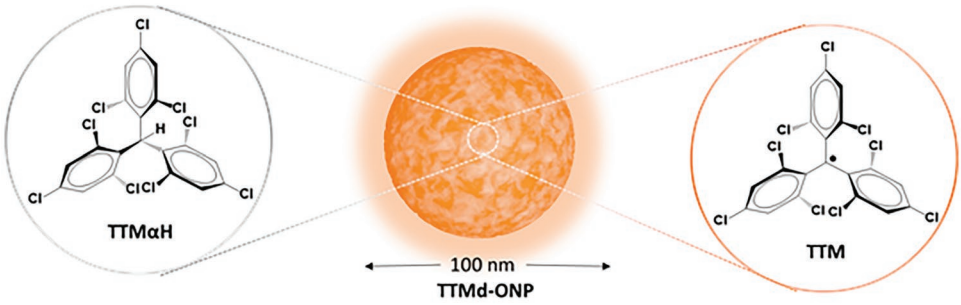

Figure 1. Molecular structures of TTM-αH and the TTM radical molecules and idealized representation of TTMd-ONPs made of a blend of TTM-αH, acting as a matrix and the optically active TTM radical.

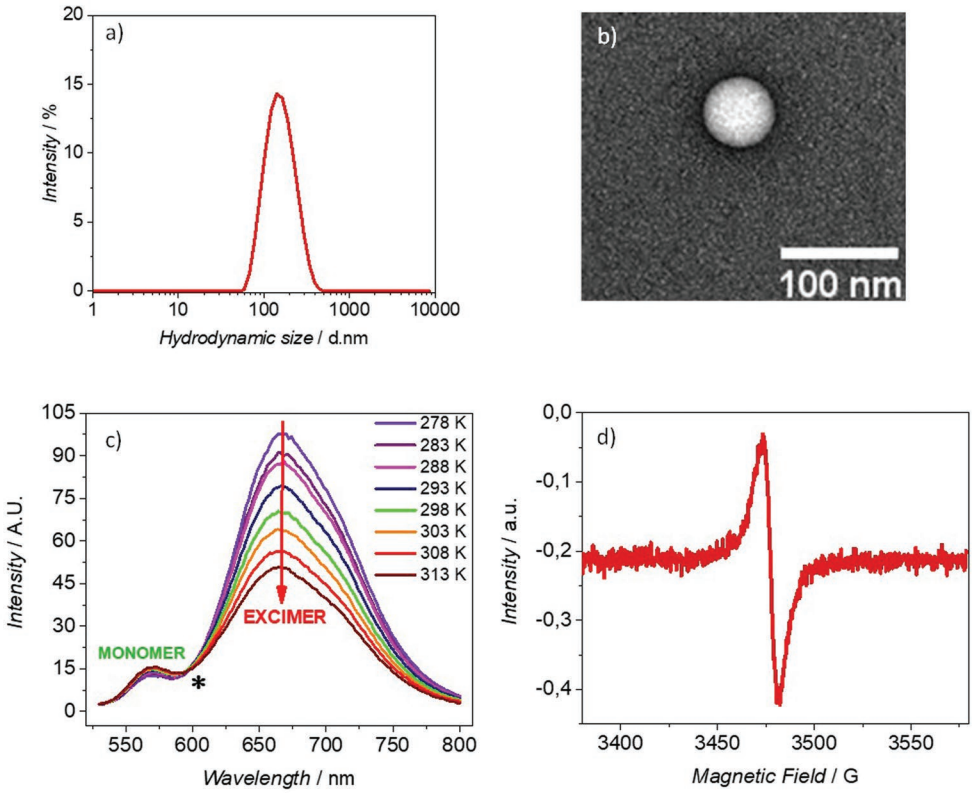

Figure 2. TTMd-ONPs 20% water suspension (with 5% in vol of THF); a) dynamic light scattering (DLS) size distribution at RT and b) representative TEM image of one TTMd-ONP; c) fluorescence emission spectra changing the temperature in the range 278 – 313 K (step 5 K). The isostilbic point is marked with an asterisk. d) EPR signal at RT.

properties of TTM radical doped ONPs offer outstanding opportunities as contactless nanothermometer. To accomplish such objective, we started investigating the TTMd-ONPs composed of 20% w/w of TTM radical dispersed in the TTM-αH matrix. These ONPs were prepared by slow dropping of a THF solution of the two mixed molecules into MilliQ water as reported.[36,37] The resulting water suspension of ONPs (with 5% in vol of THF), showed an average hydrodynamic diameter of 100 nm with negative Z-potentials close to –45 mV (**Figure 2**a). Figure 2 shows the emission spectra of these particles as a function of temperature in the 278 –313 K range. The excimer emission at 665 nm is strongly quenched upon increasing the temperature, while the monomer emission at 572 nm is weakly affected by the thermal variation. The system exhibits an isostilbic point at 594 nm clearly indicating a temperature-controlled equilibrium between monomers and excimers (Figure S1a, Supporting Information). Moreover, electron paramagnetic resonance (EPR) measurements of TTMd-ONPs (Figure 2d) demonstrate that the radical magnetic properties are preserved inside the nanoparticles.

Figure 3a,b shows the absorption spectra of water suspension of TTMd-ONPs and the temperature-dependence of the excimer (orange) and monomer (blue) maximum emission intensities. Interestingly, as it can be seen following the temperature-dependence of the luminescent intensity ratio, LIR = I_M/I_E, the process is completely reversible (Figure 3c; Figure S1b, Supporting Information), so collections of TTMd-ONPs can be used to monitor real-time temperature variations of their suspensions. We already observed in our previous work that changing the TTM doping concentration in ONPs, allows tuning both the monomer/excimer fluorescence intensity ratio and the maximum wavelength of the excimer emission band, which is red-shifted upon increasing the radical concentration.[25,36,37] For this reason, ONPs with different % of doping were prepared (15, 20, 25% w/w of TTM) and the resulting suspensions of ONPs in water with a 5% of THF showed average sizes and Z-potentials values of 100 nm, with narrow size distribution, and –45 mV, respectively.

The thermometric parameter I_M/I_E at different temperatures were fitted with the empirical Equation (1).[25,39,40]

$$\mathrm{LIR} = \frac{I_M}{I_E} = a + b\exp(cT) \quad (1)$$

where I_M and I_E correspond to the maximum intensity of fluorescence emission of the monomer and excimer respectively, and a, b, and c are constants.

To determine the performance of the nanothermometric system we evaluated the luminescent intensity ratio (LIR) and compare the results with other reported sensors determining the absolute sensitivity (S_a), using Equation S1 (Supporting Information).

However, to compare LIR of systems, that are different in nature, it is preferable to use the relative sensitivity (S_r)

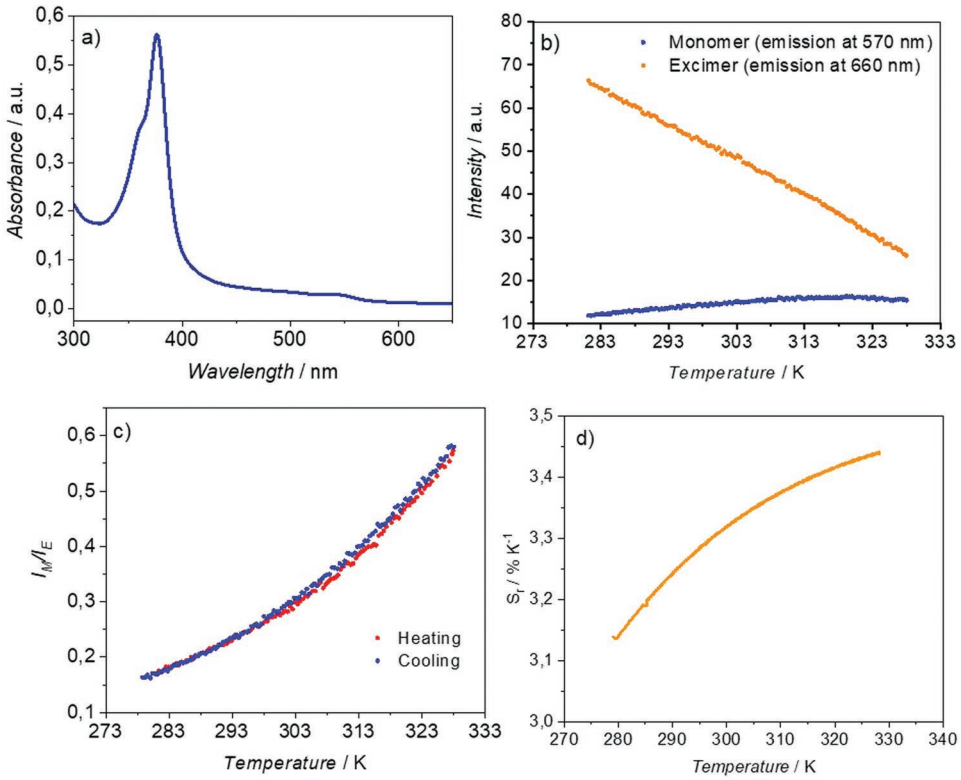

Figure 3. TTMd-ONPs 20% water suspension (with a 5% of THF); a) absorption spectrum, b) temperature-dependent excimer (orange) and monomer (blue) maximum emission intensities, c) luminescent intensity ratio of monomer over excimer in one cycle heating/cooling showing the high reversibility of temperature sensing of the ONPs and d) relative sensitivity of the particles with increasing temperature.

parameter and not the absolute sensitivity (S_a) value, given by Equation (2).[25,39,40]

$$S_r = \left|\frac{\partial Q / \partial T}{Q}\right| \times 100\%, \ [\%\cdot K^{-1}] \quad (2)$$

Temperature dependence of ratiometric output $Q(T)$ was obtained by fitting the experimental I_M/I_E ratio with the empirical Equation (1), for the three TTMd-ONPs samples (Figure S2, Supporting Information). Afterwards, to evaluate the performance of every sample as nanothermometer, it was calculated the values of the absolute and relative sensitivity, using Equations S1 (Supporting Information) and 2, respectively (Figure S2, Supporting Information). TTMd-ONPs with 20% of TTM exhibited the best relative sensitivity all along the investigated temperature range, showing a thermal relative sensitivity at RT of S_r = 3.3%K^{-1} (T = 298 K); one of the highest values reported for nanothermometers based on small fluorescent metal-free organic molecules using an intensity-based method for the thermal detection.[41] The smallest detectable temperature change or minimum temperature resolution was estimated, using Equation S2 (Supporting Information), as ΔT_{min} = 0.3 degree, which is very good compared with other reported systems.[8,42] Hence, 20% TTMd-ONPs suspension was chosen as the optimal suspension for further studies (Figure 3).

To use the TTMd-ONPs as contactless nanothermometers for bio-sensing, the suspension was dialyzed to remove the remaining organic solvent (THF), present due to particle preparation. Dialysis caused a small reduction of the relative sensitivity since ONPs dispersed in pure MilliQ water showed a S_r = 2.3% K^{-1} (T = 298 K) (Figure S3, Supporting Information). This sensitivity change is attributed to the elimination of THF traces that may be trapped into the ONPs during the self-assembly process. It is remarkable, that above 283 K the sensitivity remains above 2% K^{-1}, which is a very promising result considering the generally accepted value of 0.5% K^{-1} quality threshold for useful biosensing nanothermometers,[25] which is exceed by our ONPs in the whole temperature range. The effect of the dialysis did not affect the ONPs morphology, size, or size distribution. Thus, ONPs presented a uniform monomodal size distribution, with an average diameter of 106 ± 21 nm (Figure S4, Supporting Information), a Z-potential of –42 mV and a spherical shape, exactly as observed for samples after preparation.[37]

To move on toward biological applications of 20% TTMd-ONPs as nanothermometers, their spectroscopic and colloidal properties were tested in conditions more similar to those of intracellular and biological environments. First, we verified that the ratiometric output or LIR thermometric parameter of TTMd-ONPs suspensions is independent of concentration fluctuations because this issue is fundamental in bio-imaging since ONPs could accumulate differently in specific areas of the analyzed cells or tissues. With this aim, the thermometric parameter of 20% TTMd-ONPs in pure MilliQ water was compared with the 1:3 dilution (20% TTMd-ONPs dil). Results in Figure S5 (Supporting Information) demonstrate that both

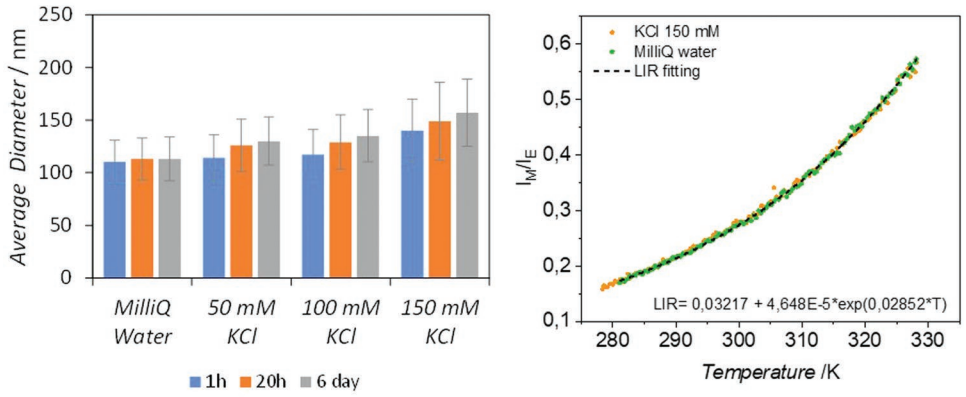

Figure 4. Effect of the ionic strength on the optical and colloidal properties of 20% TTMd-ONPs water suspensions. KCl was added in three concentrations: 50, 100, and 150 mM. Left) Size stability by DLS; right) stability of fluorescence intensity ratios as a function of temperature.

suspensions exhibit the same ratiometric output and sensitivity. The effect of the ionic strength on the optical and colloidal properties was also analyzed because it is well known that the presence of salts can affect the colloidal stability of the suspensions enhancing aggregation of ONPs with concomitant optical changes. The most abundant ion in the cytoplasm is potassium, with a concentration of ≈139 mM.[27] Thus, in order to evaluate the effect of the K^+ ion on the optical properties and the colloidal stability of 20% TTMd-ONPs suspensions, KCl was added in a fresh-dialyzed sample in three different concentrations: 50, 100, and 150 mM. The three resulting suspensions and the suspension in pure MilliQ water were analyzed by dynamic light scattering (DLS) technique at 1 h, 20 h, and 6 days after the addition of the potassium salt, and the results are reported in **Figure 4**. In pure water, the system is extremely stable and no appreciable changes occur during six days; a result that can be ascribed to the highly negative values of the Z-potential of ONPs preventing their aggregation. Adding higher amounts of KCl salt slightly destabilizes the suspensions, but small signals of aggregation can be observed only after six days with the largest salt concentration of 150 mM assayed. Nevertheless, no changes in the optical response of the ONPs were associated with this aggregation since the fluorescence intensity rations of the sample in MilliQ water and the one with KCl at 150 mM, after six days are not significantly different (Figure 4). This result shows that suspensions of a collection of isolated ONPs and those with some degree of aggregation exhibit the same emissive properties.

Another key parameter to consider for biosensing applications of ONPs is the pH. The regulation of the pH is a fundamental process for cell's correct growth and function. Indeed, cellular metabolic activities, with CO_2 and lactic acid production, can modify the intracellular pH-inducing complex H_3O^+ transporting processes.[43–45] Consequently, the optical properties and colloidal stability of 20% TTMd-ONPs suspensions were tested in the range of pH 5–8 using phosphate-buffered saline (PBS) solutions (Table S1, Supporting Information). Analyzing the DLS data of suspensions at three different pH values during 4 days (Figure S6, Supporting Information), shows that the most acidic media (pH 5) promotes a small aggregation of the particles after 4 days, while the suspension at pH 8 does not show any signal of aggregation. This result is consistent with the fact that ONPs present a negative value of Z-potential. Also, in this case, the I_M/I_E luminescent intensity ratios of the three suspensions are not significantly different.

As the last physicochemical characterization, we checked the colloidal and emission stability of the 20% TTMd-ONPs suspensions after prolonged thermal stress in order to evaluate the possibility to use such nanoparticles also as nanothermometers in hyperthermia therapy. PBS was added to a fresh dialyzed sample to buffer the pH at 5.0, 6.5, and 8.0, with an ionic strength of 150 mM (Table S2, Supporting Information). The resulting suspensions together with the nanoparticles in MilliQ water were heated for 2 h at 323 K and DLS analysis was performed before heating, and after 1 h and 2 h of heating (Figure S7, Supporting Information). In MilliQ water the heating process does not induce any growth of particles while in the presence of PBS there is a slight tendency to increase particle size which is almost independent of the pH. Prolonged heating at 323 K did not induce any precipitation or drastic aggregation; thus, the 20% TTMd-ONPs is a robust system to be considered as a fluorescent nanothermometer suitable also for sensing in different environmental conditions relevant for in vivo applications, i.e., hyperthermia therapy.

To use TTMd-ONPs as nanothermometers for cellular biosensing we performed a viability assay[46] evaluating the metabolic activity of cells in the presence of 20% TTMd-ONPs suspensions using the 3-(4,-5-dimethylthiazo-l-2yl-)2,-5diphenyl-trtrazolium bromide (MTT) colorimetric assay. The obtained cell viability results with COS-7 cells, a kidney fibroblast-like cell line (Figure S8, Supporting Information), indicate that such cells are viable in all tested concentrations of ONPs. Additionally, tsa201 embryonic adherent cells, a transformed human kidney cell line, were incubated with the ONPs suspension. Fluorescence microscopy images showed healthy cell morphologies which support the good biocompatibility of the ONPs (Figure S9, Supporting Information).

Once we have demonstrated that suspensions of TTMd-ONPs are not cytotoxic and permit us to sense the temperature of their aqueous surrounding media with high sensitivity, we addressed if isolated nanoparticles might sense the local temperature at the nanoscale. We incubated 20% TTMd-ONPs suspensions at a given concentration on top of a small glass coverslip treated with poly-L-Lys for ONP attachment, which

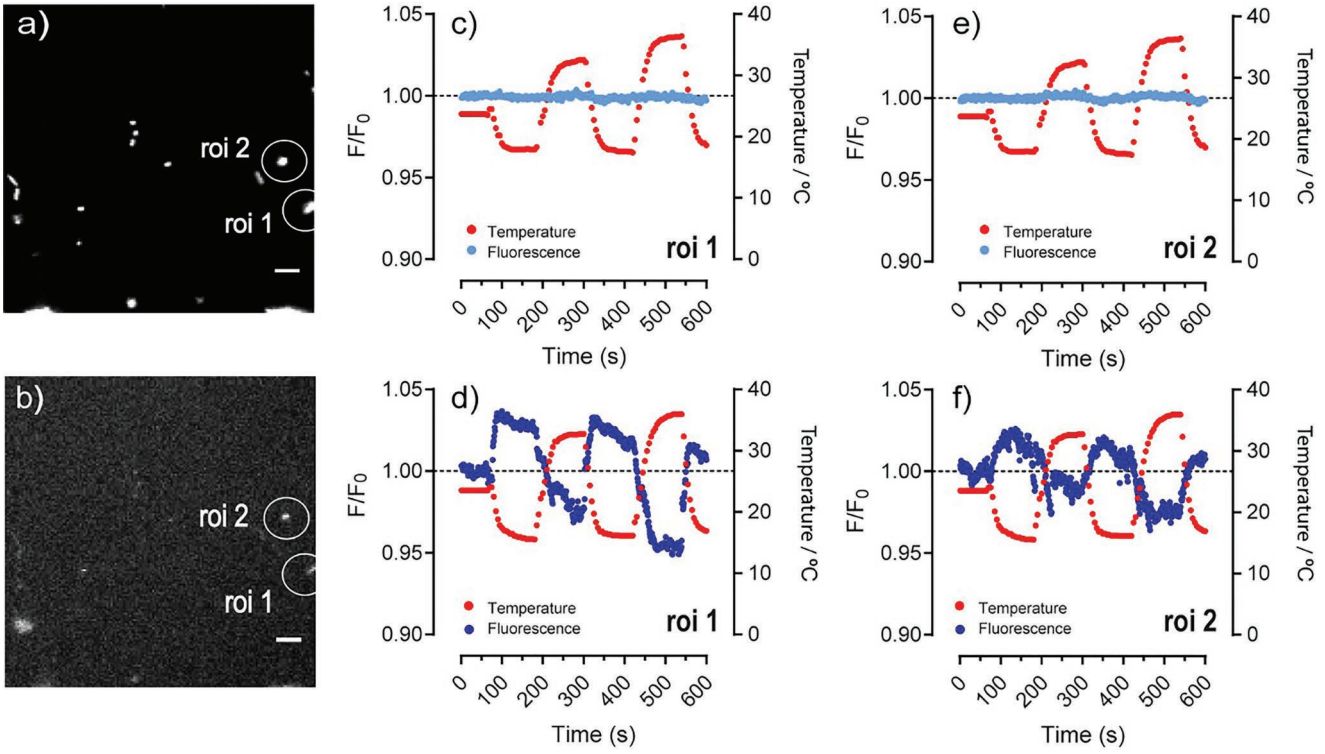

Figure 5. Representative images and fluorescence intensity versus time traces of 20% TTMd-ONPs in response to sequential temperature gradients. Images and emissive signals for ROIs #1 and # 2 were recorded with a fluorescence inverted microscope exciting at λ_{exc} = 377 nm and detecting the emission with a 510–560 nm filter for the monomers (a) and with a 595–670 nm filter for the excimers (b). Scale bar 1 µM. Variation of the fluorescence intensity ratio (F/F_0) emitted by the monomers (c,e) and by the excimers (d,f) in a temperature interval of ≈20 degrees.

was connected to a fluidic system. We placed under the coverslip a system to cool down and warm up the sample with a temperature amplitude of +/−20 degrees. To test for reversibility and homogeneity, we performed two cold-hot cycles in each measurement, choosing different regions of interest (ROIs) whose fluorescence signals were analyzed separately (**Figure 5**). To record the TTMd-ONPs fluorescence signals, we employed an inverted fluorescence microscope exciting at λ_{exc} = 377 nm (using a monochromatic light source based on a xenon lamp) and reading the emissions with two different dichroic filters: the first one at 510–560 nm recording the emission of monomers and the second one at 595–670 nm for the excimer's emission (Figure 5a,b). Interestingly, the monomer fluorescence intensities of nanoparticles in two ROIs remained almost constant in a temperature interval of ≈20 degrees (Figure 5c,e), while the excimer signals were inversely proportional to it (Figure 5d,f). This result demonstrates that TTMd-ONPs can sense temperature changes locally at the nanoscale, and behave as ratiometric temperature nanoprobes. For statistical analysis of fluorescence emission signals, see Figure S10 (Supporting Information).

After demonstrating the temperature sensing capability of 20% TTMd-ONPs at the submicron scale, we measured the temperature in living *Caenorhabditis elegans (C. elegans)* worms as an in vivo model system. *C. elegans* is a 1 mm long nematodes, with a short life cycle, rapid reproduction, optical transparency, and physiological similarity with humans.[47] Therefore, *C. elegans* offer experimental simplicity and valuable information as an animal model to test bioimaging probes,[42,48] for nanothermometry experiments using nanoparticles.[42,49,50]

Before using our ONPs in *C. elegans*, we carried out several control experiments of the ONPs´ behavior in the environment of *C. elegans*. First, we checked if the M9 buffer, the saline medium commonly used to maintain and expose ONPs to *C. elegans*, affected the hydrodynamic sizes and size distributions of the 20% TTMd-ONPs over time. During the first 24 h (time of ONPs exposure to *C. elegans*) no significant changes in the average hydrodynamic size and size distributions of ONPs occurred (Figure S11, Supporting Information). So, the nanoparticles preserve their original average diameter of ≈100 nm, which is an appropriate size to be ingested by the worms. The L4 larval stage worms were treated with 55 µg mL^{-1} suspension of 20% TTMd-ONPs in liquid M9 buffer for 24 h (**Figure 6**; Figure S12, Supporting Information). After 24 h of exposure 97% of worms were alive with no significant difference from the control group, which demonstrates that ONPs are not lethal for the worms. Similarly, we also measured body length after exposure to examine the growth and development of *C. elegans* from the L4 to the egg-bearing adult stage during the 24 h, and found that the ONPs did not affect the rate of development significantly. The survival and development assays confirm that the TTMd-ONPs do not show any biological toxicity in *C. elegans*. A third control experiment was employed to determine the survival rate of *C. elegans* at different temperatures. This test helped to identify at which temperature the worms died to determine the temperature range to use the worms as

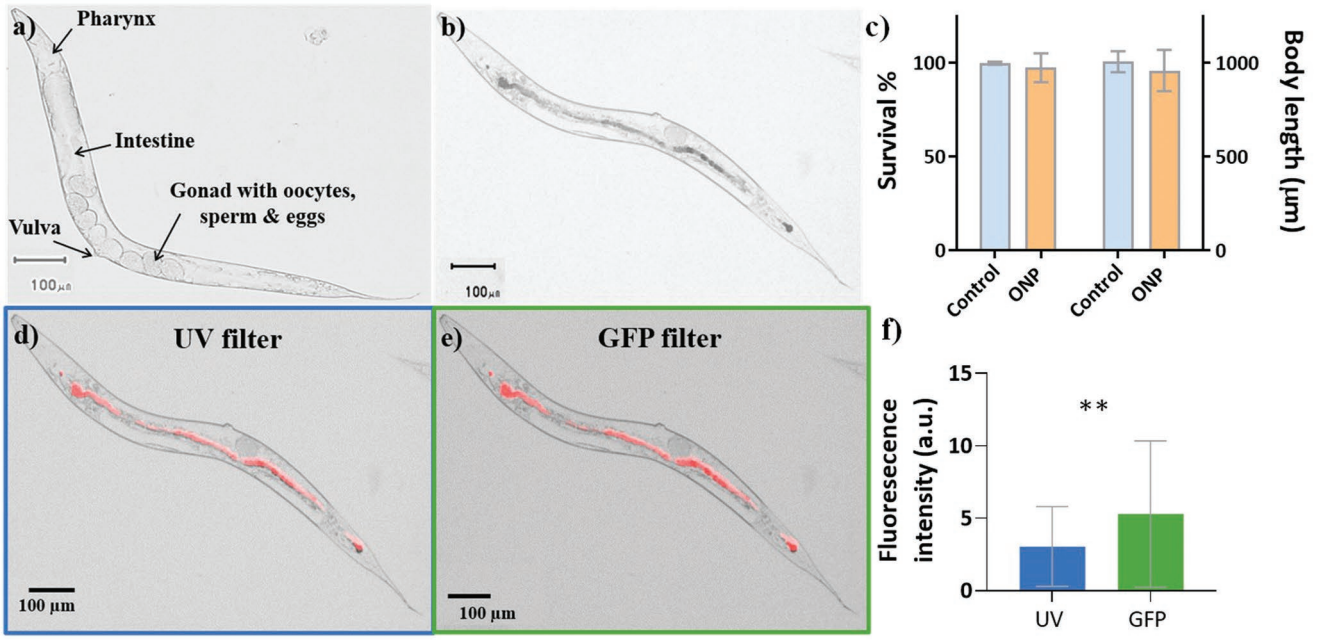

Figure 6. a) Untreated control *C. elegans* where some anatomical parts of the worm are described; b) *C. elegans* treated with ONPs. c) Survival rate and body length of *C. elegans* with and without ONPs. Treated worms under d) UV filter (>510 nm), e) GFP filter (>590 nm), where the TTM-ONPs are visualized in the intestine; f) comparative fluorescence intensity of ONPs under the two filters.

a model system to test the TTMd-ONPs as nanothermometers. *C. elegans* were heated up with steps of 5 K starting from 293 until 328 K. For each temperature, after two minutes of stabilization, a few drops of the worms' suspension were observed under the microscope to count the dead and alive worms. The survival rate at 293 K was considered as the positive control since some worms could have died for other reasons. Table S3 (Supporting Information) shows survival rates obtained in the studied temperature range, showing that, at 308 K, 72% of worms were still alive which declined drastically at temperatures higher than 313 K (Figure S13, Supporting Information). This result indicates that *C. elegans* can be used as an in vivo model system for validating ONPs as nanothermometers but only at temperatures below 313 K.

Then, we proceeded to observe the *C. elegans* exposed to 55 µg mL^{-1} of the 20% TTMd-ONPs with a fluorescence microscope using UV (> 510 nm) and Green (> 590 nm) long pass filters at RT to visualize ingested ONPs (Figure 6). The ONPs were ingested orally and passed through the pharynx to the intestines. Higher accumulation of ONPs can be observed near the pharynx since it acts as a filter-grinder and ONPs might concentrate there.[51]

After visualizing the nanoparticles within the worms, the output emission intensity of the ONPs was measured to check the validity of the luminescent ONPs as an in vivo nanothermometer. Taking advantage of the transparency of the worms, we proceeded in the same way as with the 20% TTMd-ONPs aqueous suspensions, measuring the emission of a suspension of *C. elegans* exposed to ONPs and control *C. elegans* in a cuvette. We compared the emission spectra of a suspension of *C. elegans* with a suspension of *C. elegans* exposed to ONPs at 278 and 298 K (Figure S14, Supporting Information). Interestingly, in the untreated *C. elegans* suspension, an emission band at 523 nm appears when the worms are alive which is attributed to their tissue autofluorescence, that overlaps with the monomer band of the ONPs.[52] The intensity of this band increases significantly when the sample is heated at 328 K and remains intense when the suspension was cooled down to 278 K. Indeed, the increase of this band has been attributed to the death of the worms with the temperature and the denaturation of proteins.[53] In the literature, a model predicts that 1% of the *C. elegans* proteome should be denatured at 320 K and 50% of their proteome is denatured at 326 K.[54] These results indicate that *C. elegans* cannot be used as model systems for evaluating in vivo the performances of ONPs as nanothermometers at temperatures higher than 313 K.

Finally, to determine the sensitivity of 20% TTMd-ONPs inside the worms as nanothermometers and to compare it with the free nanoparticles, further emission spectra were performed. For both suspensions, an emission scan was performed at 278 K with an excitation wavelength of 377 nm to obtain the maxima of the monomer and excimer emission bands of the TTMd-ONPs in the two samples. Then, a thermal scan was performed, recording only the maximum intensity for the excimer and monomer bands, every 0.5 K, from 278 K until 313 K with a heating rate of 0.8 K min^{-1}. Finally, to check the reversibility of the system the inverse thermal scan was carried out, from 313 to 278 K. The luminescence intensity ratio (Q) between the maximum of the monomer, corrected by subtracting the emission of the worms due to its autofluorescence at 523 nm, and the maximum of excimer was plotted and fitted using the LIR empirical Equation (1) through data points at different temperatures. Then, deriving the LIR function of Q with respect to temperature, the thermal absolute sensitivity

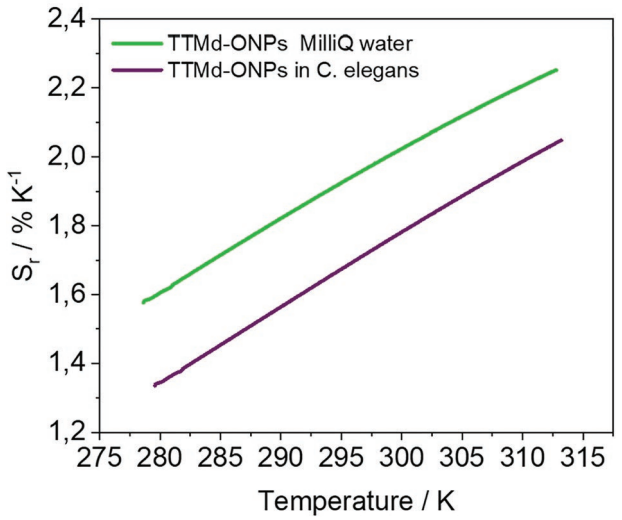

Figure 7. Relative sensitivity of TTMd-ONP as nanothermometer at different temperatures in water suspension (green) and inside *C. elegans* (violet).

values for both samples were obtained using Equation S1, and the relative sensitivity was determined using Equation (2). As observed in **Figure 7**, the sensitivity of the ONPs ingested in *C. elegans* (TTMd-ONP *C. elegans*) was successfully measured and found to be very significant, $S_r = 1.7\%\ K^{-1}$ ($T = 298$ K). The relative temperature sensitivity is always higher than 1% K^{-1} in the whole evaluated temperature range, which is twice the threshold quality value of 0.5% K^{-1} set in the literature for nanothermometry applications.[25] In addition we also estimated a minimum temperature resolution of $\Delta T_{min} = 0.6$ degrees, using Equation S2 (Supporting Information), which is also a very promising result for future applications of TTMd-ONPs as in vivo fluorescent nanothermometers.

The possibility to measure changes of temperature dependent fluorescence emission, of organic nanoparticles in a live organism is very promising, but to use them in practical applications, it is necessary to show the performance of this nanothermometer locally at the submicron scale. Hence, we have measured temperature changes inside individual *C. elegans* in a localized area of their intestine, using a confocal microscope. For confocal measurements, *C. elegans* were immobilized using NemaGel, and changes in temperature were recorded by tracking the fluorescence emission intensity at two wavelength ranges, 420–570 and 620–720 nm to record the emission associated with the monomer and the excimer, respectively. A 3D representation of the *C. elegans* intestine with the ingested TTMd-ONPs is represented in Figure S15 (Supporting Information) with also a zoom of a small area showing emission of monomer (green) and excimer (red) of a single TTMd-ONPs particle/aggregate.

Three different temperature ranges were studied starting from 290–293 K by cooling the microscope cage with dry ice, then increasing it to 297–300 K and finally to 307–308 K, by using a heater coupled to the confocal. For each temperature at least 6 measurements were recorded to have statistical data. In **Figure 8**a is represented the ratio between monomer and excimer emission in the bottom region of the intestine of the *C. elegans*, the data for the top region is represented in Figure S16 (Supporting Information).

As demonstrated above, with increasing temperature, the ratio between the monomer and excimer emissions bands (Q) increases and the same behavior is shown locally inside an individual *C. elegans*. These results demonstrate that these ONPs can be used to measure the temperature in a small localized area of a single animal.

Even though the deviation for each temperature range is broad because every *C. elegans* is different and can metabolize the TTMd-ONPs in different ways, similar ratiometric behavior to that obtained in vitro is observed. When increasing the temperature, the fluorescence emission intensity decreases for the red frame (420–570 nm) and keeps constant for the green one (620–720 nm). For a better understanding of the data, Figure 8b shows the same *C. elegans* animal at two different temperatures. At higher temperature a decrease of fluorescence intensity of the nanoparticles at higher wavelengths is observed, supporting the reported data.

3. Conclusion

We have developed organic radical TTMd-ONPs, as ratiometric nanothermometers based on a radical excimer for in vivo sensing with excellent temperature sensitivity 3.4% K^{-1} (at 328 K), reversibility and high colloidal stability. One of the advantages of the described system is its simplicity since both the host and guest molecules forming the nanoparticles are small metal-free organic molecules which allow higher control on the molecular structure, higher reproducibility of the synthesis, and easier purification than polymers. Moreover, both the host and the guest molecules, the TTM-αH and TTM radical, respectively, are processed as nanoparticles by the self-assembly of the two molecules in a simple single-step process using the re-precipitation method. Thanks to the simplicity of the synthesis of the two molecules and their self-assembly properties, TTMd-ONPs constitute an example of a cost-effective thermal sensor. In pure water the suspension of TTMd-ONPs is colloidally stable offering the possibility to be stored for a long time without aggregation or radical-leaking phenomena. The colloidal properties are preserved even increasing the ionic strength and varying the pH in the range of 5 – 8. Furthermore, TTMd-ONPs show two emission bands with a ratiometric output or LIR thermometric parameter, that is independent of dilution, particle aggregation, ionic strength, and pH, while was strongly affected by changes in temperature, showing a completely reversible behavior without any hysteresis. The second strength of TTMd-ONPs is provided by the open-shell electronic configuration of the TTM radical emitter molecule, present as a monomer or as an excimer, which ensures better optical performances than close-shell fluorophores. Indeed, sensors based on organic closed-shell fluorophores show low values of Stokes shift and short lifetimes (≈ ns), which make these systems subjected to use inner-filter effects and showing scattering problems. Thanks to the large Stokes shift and their large emission lifetime (for both the monomer and the excimer emission) TTMd-ONPs can avoid problems related to the autofluorescence of the biological tissue or the scattering of the

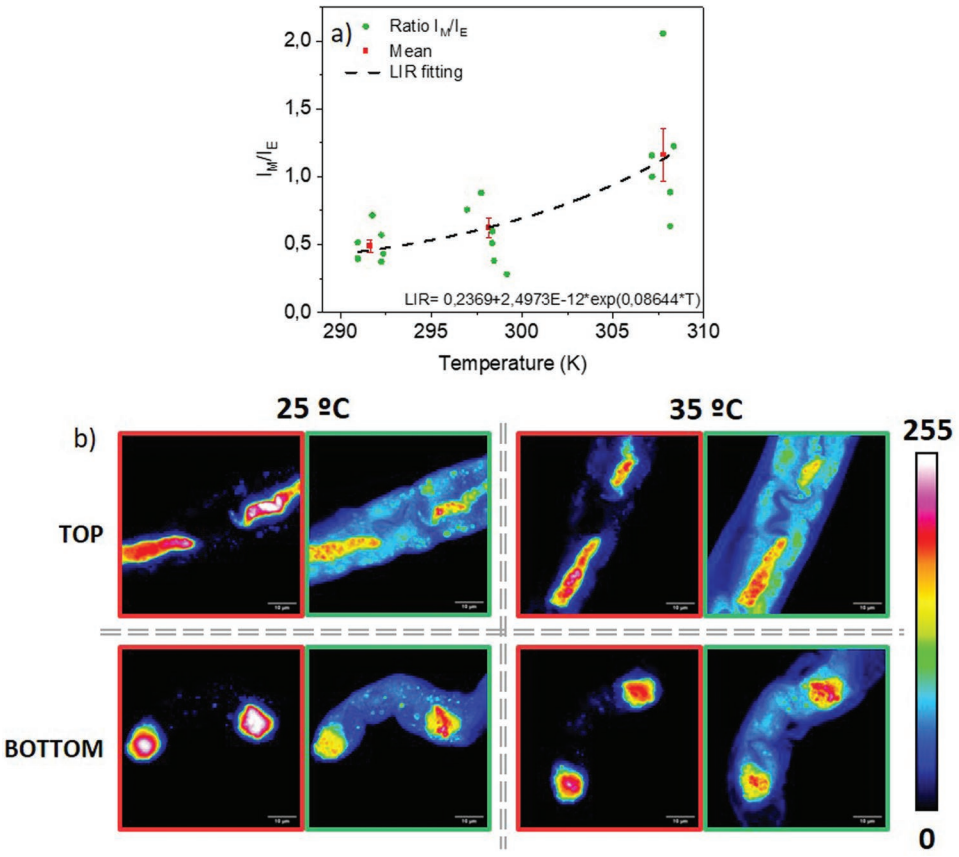

Figure 8. a) Local measurement of the ratio (Q) I_M/I_E between monomer and excimer maxima fluorescence emission at increasing temperature of the TTMd-ONPs inside *C. elegans*, from a region of the bottom of the body. Red points represent the average of the ratios and the error bars are the standard errors caused by different worms for the same temperature range, for $n = 6$ and p = 0.9917, 0.9994, and 0.9959, respectively; b) representative confocal images of the top and bottom parts from the same *C. elegans* with TTMd-ONPs inside the intestine at two different temperatures, 298 K (left) and 308 K (right). The green frame represents the 420–570 nm detection wavelength and the red frame the 620–720 nm wavelength. Scale bar 10 μM. The color scale shows pixels with the lowest intensity (0) to the highest intensity (4095).

excitation light. Since simply applying a delay between the excitation and the detection it is possible to considerably increase the signal to noise ratio. Therefore, TTMd-ONPs constitute a small-molecule-based luminescence ratiometric sensor able to join the strengths of both organic and inorganic sensors but being all-organic. TTMd-ONPs emit in the region of deep-red/NIR (i.e., the first transparency windows of biological tissues), offering the opportunity to obtain a deep-tissue penetration for in vivo applications. In addition, TTMd-ONPs are not cytotoxic and their ratiometric outputs are unaffected by changes of small aggregations, pH or ionic strength that may occur under physiological conditions. Finally, in vivo thermometry experiments made with *Caenorhabditis elegans* worms indicated that TTMd-ONPs could monitor locally in vivo the temperature changes at the sub-micron scale from 278 to 313 K, with a high sensitivity indicating the considerable potential applications of TTMd-ONPs in the biological thermometry field. In addition, thanks to the chiroptical and magnetic properties of polyhalogenated trityl radicals,[55,56] new nanothermometers are being designed, enhancing the optical outputs and versatility of these systems for biological and clinical research.[57] Moreover, to use these systems in a biological environment, both, the excitation and the emission wavelength are required to be in the biological window. In a work in progress we are studying the use of TTMd-ONPs as two-photon microscopy probe to increase the excitation wavelength in order to have both the excitation and the emission wavelengths in the biological window increasing its penetration capacity into tissues and cells without damage.

Supporting Information

Supporting Information is available from the Wiley Online Library or from the author.

Acknowledgements

D.B. and N.G.-P. contributed equally to this work. The authors are grateful for the financial support received from the Spanish Government (PID2020-115296RA-I00, PID2019-105622RB-I00, PDI2021-122645OB-I00, RTI2018-096273-B-I00 and PID2019-111493RB-I00) funded by MICIN and the "Ramón y Cajal" program (RYC-2017-22614), the Generalitat de Catalunya (SGR-918, 2017SGR765, SGR Cat 2021-00438, 2017-SGR-1442, and 2021-SGR-1410, 2021-SGR-00446), and the Networking Research Center on Bioengineering, Biomaterials, and Nanomedicine (CIBER-BBN). DB gratefully acknoledges the REFIN (Return for Future

Innovation) action for funding, an ininitiative co - funded by European Union through the POR Puglia 2014 - 2020 (ID grant: 2455F798). This research was also supported by the European Union's Horizon 2020 research and innovation program H2020-MSCA-COFUND-2016 (DOC-FAM, grant agreement Nr. 754397), Human Brain Project WaveScaES (SGA2-785907 and SGA3-945539), DEEPER (ICT36-2020-101016787), and the Marie Skłodowka-Curie grant agreement Nr. 101007804 (Micro4Nano). Support from Fundaluce and CaixaHealth (ID 100010434) are also acknowledged. The work was supported as well by the Max Planck Society through the Max Planck Partner Group "Dynamic Biomimetics for Cancer Immunotherapy" in collaboration with the Max Planck for Medical Research (Heidelberg, Germany). ICMAB-CSIC acknowledges support from the Severo Ochoa Programme for Centres of Excellence in R&D (FUNFUTURE, CEX2019-000917-S). IBEC acknowledges support from the CERCA programme of AGAUR/ Generalitat de Catalunya and the Severo Ochoa Programme. This work had been developed inside the "Biochemistry, Molecular Biology and Biomedicine" and "Materials Science" Ph.D. programs of UAB. Nerea Gonzalez-Pato acknowledges the financial support from the FPU fellowship (FPU17/02551) from the Spanish Ministry.

Conflict of Interest

The authors declare no conflict of interest.

Data Availability Statement

The data that support the findings of this study are available from the corresponding author upon reasonable request.

Keywords

Caenorhabditis elegans, excimer emission, in vivo sensing, luminescence, organic radical nanoparticles, ratiometric nanothermometers, trityl radicals

Received: December 13, 2022
Revised: March 24, 2023
Published online:

[1] A. Majumdar, *Annu. Rev. Mater. Sci.* **1999**, *29*, 505.
[2] D. Halbertal, J. Cuppens, M. B. Shalom, L. Embon, N. Shadmi, Y. Anahory, H. R. Naren, J. Sarkar, A. Uri, Y. Ronen, Y. Myasoedov, L. S. Levitov, E. Joselevich, A. K. Geim, E. Zeldov, *Nature* **2016**, *539*, 407.
[3] M. Tzur, B. Desiatov, I. Goykhman, M. Grajower, U. Levy, *Opt. Express* **2013**, *21*, 29195.
[4] O. Yarimaga, S. Lee, D. Y. Ham, J. M. Choi, S. G. Kwon, M. Im, S. Kim, J. M. Kim, Y. K. Choi, *Macromol. Chem. Phys.* **2011**, *212*, 1211.
[5] K. Okabe, N. Inada, C. Gota, Y. Harada, T. Funatsu, S. Uchiyama, *Nat. Commun.* **2012**, *3*, 705.
[6] G. Kucsko, P. C. Maurer, N. Y. Yao, M. Kubo, H. J. Noh, P. K. Lo, H. Park, M. D. Lukin, *Nature* **2013**, *500*, 54.
[7] K. Okabe, R. Sakaguchi, B. Shi, S. Kiyonaka, *Pflugers Arch. Eur. J. Physiol.* **2018**, *470*, 717.
[8] J. Zhou, B. del Rosal, D. Jaque, S. Uchiyama, D. Jin, *Nat. Methods* **2020**, *17*, 967.
[9] M. Monti, L. Brandt, J. Ikomi-Kumm, H. Olsson, *Scand. J. Haematol.* **1986**, *36*, 353.
[10] E. N. Cerõn, D. H. Ortgies, B. Del Rosal, F. Ren, A. Benayas, F. Vetrone, D. Ma, F. Sanz-Rodríguez, J. G. Solé, D. Jaque, E. M. Rodríguez, *Adv. Mater.* **2015**, *27*, 4781.
[11] L. Meng, S. Jiang, M. Song, F. Yan, W. Zhang, B. Xu, W. Tian, *ACS Appl. Mater. Interfaces* **2020**, *12*, 26842.
[12] H. Zhou, M. Sharma, O. Berezin, D. Zuckerman, M. Y. Berezin, *ChemPhysChem* **2016**, *17*, 27.
[13] M. Quintanilla, M. Henriksen-Lacey, C. Renero-Lecuna, L. M. Liz-Marzán, *Chem. Soc. Rev.* **2022**, *51*, 4223.
[14] J. M. Lupton, *Appl. Phys. Lett.* **2002**, *81*, 2478.
[15] N. Chandrasekharan, L. A. Kelly, *J. Am. Chem. Soc.* **2001**, *123*, 9898.
[16] V. A. Vlaskin, N. Janssen, J. Van Rijssel, R. Beaulac, D. R. Gamelin, *Nano Lett.* **2010**, *10*, 3670.
[17] S. Rohani, M. Quintanilla, S. Tuccio, F. De Angelis, E. Cantelar, A. O. Govorov, L. Razzari, F. Vetrone, *Adv. Opt. Mater.* **2015**, *3*, 1606.
[18] X. Wang, Q. Liu, Y. Bu, C. S. Liu, T. Liu, X. Yan, *RSC Adv.* **2015**, *5*, 86219.
[19] J. Li, C. Sun, R. Shen, X. Cao, B. Zhou, D. Bai, H. Zhang, *J. Am. Chem. Soc.* **2014**, *136*, 11050.
[20] A. A. Tseng, K. Chen, C. D. Chen, K. J. Ma, *IEEE Trans. Electron. Packag. Manuf.* **2003**, *26*, 141.
[21] C.-W. Tseng, D.-C. Huang, Y.-T. Tao, *ACS Appl. Mater. Interfaces* **2012**, *4*, 5483.
[22] H. Zhang, J. Jiang, P. Gao, T. Yang, K. Y. Zhang, Z. Chen, S. Liu, W. Huang, Q. Zhao, *ACS Appl. Mater. Interfaces* **2018**, *10*, 17542.
[23] J. Daniel, F. Vetrone, *Nanoscale* **2012**, *4*, 4301.
[24] T. Barilero, T. L. Saux, C. Gosse, L. Jullien, *Anal. Chem.* **2009**, *81*, 7988.
[25] C. D. S. Brites, P. P. Lima, N. J. O. Silva, A. Millán, V. S. Amaral, F. Palacio, L. D. Carlos, *Nanoscale* **2012**, *4*, 4799.
[26] L. Jethi, M. M. Krause, P. Kambhampati, *J. Phys. Chem. Lett.* **2015**, *6*, 718.
[27] C. Gota, K. Okabe, T. Funatsu, Y. Harada, S. Uchiyama, *J. Am. Chem. Soc.* **2009**, *131*, 2766.
[28] S. Sinha, Z. Kelemen, E. Hümpfner, I. Ratera, J. P. Malval, J. P. Jurado, C. Viñas, F. Teixidor, R. Núñez, *Chem. Commun.* **2022**, *58*, 4016.
[29] X. Bai, W. Tan, A. Abdurahman, X. Li, F. Li, *Dyes Pigm.* **2022**, *202*, 110260.
[30] D. Mesto, Y. Dai, C. N. Dibenedetto, A. Punzi, J. Krajčovič, M. Striccoli, F. Negri, D. Blasi, *Euro. J. Org. Chem.* **2023**, *26*, 202201030.
[31] I. Ratera, J. Vidal-Gancedo, D. Maspoch, S. T. Bromley, N. Crivillers, M. Mas-Torrent, *J. Mater. Chem. C* **2021**, *9*, 10610.
[32] K. Kato, S. Kimura, T. Kusamoto, H. Nishihara, Y. Teki, *Angew. Chem., Int. Ed.* **2019**, *58*, 2606.
[33] S. Kimura, T. Kusamoto, S. Kimura, K. Kato, Y. Teki, H. Nishihara, *Angew. Chem., Int. Ed.* **2018**, *57*, 12711.
[34] A. Jana, L. Bai, X. Li, H. Ågren, Y. Zhao, *ACS Appl. Mater. Interfaces* **2016**, *8*, 2336.
[35] X. He, X. Shen, D. Li, Y. Liu, K. Jia, X. Liu, *ACS Appl. Bio Mater.* **2018**, *1*, 520.
[36] D. Blasi, *Molecular and Supramolecular Strategies for Highly Luminescent Trityl Radicals and Their Sensing Applications*, **2017**.
[37] D. Blasi, D. M. Nikolaidou, F. Terenziani, I. Ratera, J. Veciana, *Phys. Chem. Chem. Phys.* **2017**, *19*, 9313.
[38] J. Mérian, J. Gravier, F. Navarro, I. Texier, *Molecules* **2012**, *17*, 5564.
[39] M. Jia, Z. Sun, M. Zhang, H. Xu, Z. Fu, *Nanoscale* **2020**, *12*, 20776.
[40] H. Xu, M. Jia, Z. Wang, Y. Wei, Z. Fu, *ACS Appl. Mater. Interfaces* **2021**, *13*, 61506.
[41] Y. Sun, M. Fu, M. Bian, Q. Zhu, *Biotechnol. Bioeng.* **2023**, *120*, 7.
[42] M. Fujiwara, S. Sun, A. Dohms, Y. Nishimura, K. Suto, Y. Takezawa, K. Oshimi, L. Zhao, N. Sadzak, Y. Umehara, Y. Teki, N. Komatsu, O. Benson, Y. Shikano, E. Kage-Nakadai, *Sci. Adv.* **2020**, *6*, eaba9636.
[43] J. Kurkdjian, A. Guern, *Annu. Rev. Plant Physiol. Plant Mol. Biol.* **1989**, *40*, 271.

[44] A. Hulikova, A. L. Harris, R. D. Vaughan-Jones, P. Swietach, *J. Cell. Physiol.* **2013**, *228*, 743.
[45] T. Bagar, K. Altenbach, N. D. Read, M. Benčina, *Eukaryotic Cell* **2009**, *8*, 703.
[46] Ö. S. Aslantürk, in *Genotoxicity – A Predictable Risk to Our Actual World*, (Eds: M. L. Larramendy, S. Soloneski) IntechOpen, London **2018**, https://doi.org/10.5772/interopen.69556.
[47] L. Gonzalez-Moragas, A. Roig, A. Laromaine, *Adv. Colloid Interface Sci.* **2015**, *219*, 10.
[48] J. Chen, C. Guo, M. Wang, L. Huang, L. Wang, C. Mi, J. Li, X. Fang, C. Mao, S. Xu, *J. Mater. Chem.* **2011**, *21*, 2632.
[49] T. Kimata, H. Sasakura, N. Ohnishi, N. Nishio, I. Mori, *Worm* **2012**, *1*, 31.
[50] J. S. Donner, S. A. Thompson, C. Alonso-Ortega, J. Morales, L. G. Rico, S. I. C. O. Santos, R. Quidant, *ACS Nano* **2013**, *7*, 8666.
[51] Z. F. Altun, D. Hall, *Alimentary System, Pharynx, in Worm Atlas* **2009**, http://dx.doi.org/doi:10.3908/wormatlas.1.3.
[52] Z. Pincus, T. C. Mazer, F. J. Slack, *Aging* **2016**, *8*, 889.
[53] D. Jones, E. P. M. Candido, *J. Exp. Zool.* **1999**, *284*, 147.
[54] K. Ghosh, K. Dill, *Biophys. J.* **2010**, *99*, 3996.
[55] P. Mayorga-Burrezo, V. G. Jiménez, D. Blasi, T. Parella, I. Ratera, A. G. Campaña, J. Veciana, *Chem. – Eur. J.* **2020**, *26*, 3776.
[56] P. Mayorga Burrezo, V. G. Jiménez, D. Blasi, I. Ratera, A. G. Campaña, J. Veciana, *Angew. Chem., Int. Ed.* **2019**, *58*, 16282.
[57] C. He, H. He, J. Chang, B. Chen, H. Ma, M. J. Booth, *Light: Sci. Appl.* **2021**, *10*, 194.